Local ^{4}He-p potentials from resonating-group method phase shifts

S. G. Cooper and R. S. Mackintosh*
Physics Department, The Open University, Milton Keynes MK7 6AA, United Kingdom

A. Csótó and R. G. Lovas
Institute of Nuclear Research of the Hungarian Academy of Sciences, P.O. Box 51, Debrecen, H-4001, Hungary
(Received 25 August 1993; revised manuscript received 29 March 1994)

Phase shifts for α + nucleon scattering generated by a multichannel resonating-group method (RGM) model of the five-nucleon system are subjected to iterative-perturbative "mixed-case" inversion for energies below the reaction threshold. The resulting phase-equivalent potentials are compared with local potentials calculated from the inversion of empirical phase shifts. A strong similarity is revealed between the two sets of potentials, most notably in the description by a parity- and energy-dependent local potential. In particular, the RGM-derived and empirical potentials share a distinctive form of parity dependence in which the odd-parity component is of greater radial extent. Comparison with potentials representing single-channel RGM phase shifts exhibits the importance of the coupled channels in terms of local potentials. The relative wave functions derived from RGM are very different from those for the phase-equivalent local potentials. Connections are made with general nucleon-nucleus scattering.

PACS number(s): 21.60.Gx, 25.10.+s, 25.40.Cm, 25.40.Dn

I. INTRODUCTION

In this paper we study the relationship between empirical and microscopic nucleon-α potentials. The results are relevant to both the evaluation of the microscopic model involved [resonating-group model (RGM)] and also to understanding the general properties of the nucleon-nucleus potential. The importance of the latter lies in the fact that there are aspects of the physics of nucleon-nucleus interactions which cannot yet be generally included in studies of any but the lightest nuclei. It seems that generally speaking the "few body" and "nucleon-nucleus" literatures have almost no cross-referencing, but we do feel that they have a mutual contribution to make to each other.

The empirical potentials which enter the comparison were previously determined [1] using a two-step approach: In the first step the data are fitted by phase shifts and in the second step these phase shifts are "inverted" to yield potentials which closely reproduce them [1, 2]. The cited calculations all use the iterative-perturbative (IP) inversion method [3–6] also used in this paper and outlined in Sec. IV below.

The general question which we attempt to answer in the particular context of the mass-5 system is: Which characteristic properties of empirical local potentials are predicted by microscopic theory? The system ^{4}He+p is suitable for study for three reasons: (i) The empirical potentials have been deduced from good-quality data, (ii) they behave in a nontrivial manner, and (iii) realistic microscopic calculations, incorporating features omitted from calculations on heavier target nuclei, are feasible. In this paper, the inversion of microscopic model phase shifts yields local ^{4}He+p potentials which are compared with empirical potentials [1].

The microscopic model is the resonating-group model (RGM) with two partitions, $\{\alpha+p,^3\text{He}+d\}$ or $\{\alpha+n,t+d\}$. The local potential representing the RGM phase shifts is obtained by means of "mixed-case" inversion using the IP algorithm [3]. In mixed-case inversion [1, 2], potentials are constructed which simultaneously reproduce phase shifts for a set of angular momenta and a range of energies. The inversion is appropriate to spin-$\frac{1}{2}$ particles, and spin-orbit potentials are presented. The present calculations are concerned only with the energy range below the ^{3}He+d ($t+d$) threshold, and so all potentials are real.

Characteristic features of the empirical potential as determined by the two-step method are a strong parity-dependent *radial form* and a shorter range spin-orbit term. In order to establish whether the RGM bears out these features, one must construct the nucleon-nucleus potential corresponding to the RGM. It has long been known that exchange built into the RGM leads to parity dependence, but until now there has been no way of knowing how this should be represented in a potential model; generally it has been assumed that the shape of the potential is not parity dependent. As required by present day RGM calculations, we describe the intrinsic nuclear states by a simple model and use a schematic nucleon-nucleon interaction; the interaction is fixed for all energies and parities rather than chosen to enforce a fit at a particular energy. The fit to the data thus being modest, it is not a foregone conclusion that the nucleon-nucleus potential deduced from such a RGM behaves like the empirical potential. It must be confirmed that a presently feasible RGM does indeed encompass those aspects of microscopic dynamics responsible for the

*Electronic address: R. MACKINTOSH@OPEN.AC.UK

unexpected character of the parity dependence.

In this framework other properties of the RGM procedure can also be studied: (i) By comparing wave functions from the local and nonlocal models, we study the implications of a local representation of a nonlocal model. This is important for the application of the potential to three-body models of ^{6}He, for example. (ii) By omitting the coupling to the deuteron channel, we measure the contribution of such coupling to a ^{4}He+p potential; the corresponding calculation for heavy target nuclei, coupled reaction channel calculations of (p,d,p) effects with exchange included, is exceedingly difficult and apparently has never been performed.

II. MICROSCOPIC FORMALISM

We use an approximation to the RGM based on a generator-coordinate method (GCM). In a coupled-channel (CC) version of the model of the ^{5}Li-like system the wave function for a particular total angular momentum j and parity π is a combination of the $\alpha+p$ and $h+d$ ($h=^3$He) partitions:

$$\Psi^{\pi}_{j} = \Psi^{(\alpha p)}_{[l\frac{1}{2}]j} + \sum_{l'} \sum_{s'=\frac{1}{2},\frac{3}{2}} \Psi^{(hd)}_{[l's']j}, \tag{1}$$

where

$$\Psi^{(12)}_{[ls]j} = \mathcal{A}_{12}\left\{\left[[\Phi^{(1)}_{s_1}\Phi^{(2)}_{s_2}]_s \varphi^{(12)}_l(\mathbf{r}_{12})\right]_j\right\}, \tag{2}$$

the functions Φ are antisymmetrized intrinsic wave functions, and $\mathcal{A}_{12}$ is an interfragment antisymmetrizer.

We describe the internal motions of α and h by single translation-invariant $0s$ oscillator shell-model configurations and that of d by a combination of three such functions of different size parameters.

The nucleon-nucleon interaction in the Hamiltonian was chosen to have the form

$$V(i,j) = (\mathcal{P}_t V_t e^{-r^2/a_t^2} + \mathcal{P}_s V_s e^{-r^2/a_s^2})\tfrac{1}{2}[u + (1-u)P^r_{ij}] + (W_T + M_T P^r_{ij})r^2 \times \sum_{k=1,2} V_{\mathrm{T}_k} e^{-r^2/a^2_{\mathrm{T}_k}}[3(\boldsymbol{\sigma}_i\cdot\mathbf{r})(\boldsymbol{\sigma}_j\cdot\mathbf{r})/r^2 - \boldsymbol{\sigma}_i\cdot\boldsymbol{\sigma}_j] + V_{\mathrm{s.o.}} e^{-r^2/a^2_{\mathrm{s.o.}}}\hbar^{-1}\mathbf{l}\cdot(\boldsymbol{\sigma}_i+\boldsymbol{\sigma}_j), \tag{3}$$

where $\mathcal{P}_t$ and $\mathcal{P}_s$ are spin-triplet and -singlet projectors, respectively, P^r_{ij} is the space-exchange operator, $\mathbf{r}=\mathbf{r}_j-\mathbf{r}_i$, $\boldsymbol{\sigma}_i$ are the Pauli vectors of the nucleonic spin, and $\mathbf{l}=-\frac{1}{2}i\hbar\mathbf{r}\times(\nabla_j-\nabla_i)$ is the orbital momentum of the relative motion of the two nucleons. As in earlier work [7], we took the parameters from Blüge and Langanke [8, 9]. This interaction combines the central term of the force constructed by Chwieroth *et al.* [10] with a spin-orbit force of Reichstein and Tang [11] ($V_{\mathrm{s.o.}} = -224.8$ MeV and $a_{\mathrm{s.o.}} = 0.707$ fm) and a slightly modified version of the tensor interaction of Heiss and Hackenbroich [12]. We set the free space-exchange parameter u to 0.835 [8, 9]. The proton-proton Coulomb potential was approximated by a combination of 15 Gaussians [13]. We adopted the oscillator parameters given by Chwieroth *et al.* [10] which generate clusters of the correct size.

For each j^{π} we included all allowed combinations of $l's'$. Unlike in Ref. [7], deuteron distortion (or excitation) is not allowed for because the force parameters adopted turn out to reproduce the $\alpha+p$ empirical phase shifts at low energies better in this way. We also performed single-channel (SC) $\alpha+p$ calculations omitting the second term of Eq. (1) and carried out both CC and SC calculations for the mirror system $\alpha+n$ [14].

The RGM calculations can be tested by calculating observables directly from the S_{lj} extracted from the asymptotic form of the wave functions. However, by determining the local potential which reproduces these S_{lj} one can then apply it to, for example, mass-6 nuclei. To exploit these RGM calculations as a unique source of information concerning the effects of nonlocality, one needs the appropriate one-body nucleon-alpha wave function χ embodying the nonlocality of the RGM kernel. We shall define this, for the SC case only, as a solution of a one-body Schrödinger equation, equivalent to the RGM equation of motion, that contains a Hermitian energy-independent Hamiltonian [14, 15]. This χ is normalized as a normal one-body wave function. The nonlocal one-body potential is to be denoted by v.

III. TRIVIALLY EQUIVALENT LOCAL POTENTIALS

The microscopic potential v is nonlocal, being an integral operator of a finite-range kernel. A trivially equivalent local potential (TELP) U of a nonlocal potential v produces the same wave function χ in the local Schrödinger equation

$$(T_{\alpha p} + U)\chi = E\chi \tag{4}$$

as v in the corresponding nonlocal equation. We define two types of TELP's: one l independent and one l dependent.

We come to the l-independent TELP by taking

$$U(\mathbf{r}) \equiv V(\mathbf{r}) + iW(\mathbf{r}) = [\chi(\mathbf{r})]^{-1} v\chi(\mathbf{r}), \tag{5}$$

where $v\chi$ involves integration. Substituting U into Eq. (4) yields the one-body Schrödinger equation involving nonlocal potential v. This verifies that such a local potential yields the same relative-motion wave function χ in the entire space. It is clear that it must be complex and, through the energy dependence and boundary condition implicit in χ, it must depend on the energy and on the direction of $\mathbf{r}$. Apart from the pathological case of all partial waves having nodes at the same $\mathbf{r}$, it is not singular.

The definition (5) is identical to the definition of the ψ-

potential introduced in Ref. [16]. Indeed the function U can be cast into the form $\chi^{-1}(E-T_{\alpha p})\chi$, which implies

$$V(\mathbf{r}) = E + \frac{\hbar^2}{2\mu}\frac{\mathrm{Re}[\chi^*(\mathbf{r})\nabla^2\chi(\mathbf{r})]}{|\chi(\mathbf{r})|^2}, \tag{6a}$$

$$W(\mathbf{r}) = \frac{\hbar^2}{2\mu}\frac{\mathrm{Im}[\chi^*(\mathbf{r})\nabla^2\chi(\mathbf{r})]}{|\chi(\mathbf{r})|^2} \equiv \frac{\hbar}{2}\frac{\nabla\cdot\mathbf{j}(\mathbf{r})}{|\chi(\mathbf{r})|^2}, \tag{6b}$$

where μ is the reduced mass of the fragments and $\mathbf{j}(\mathbf{r})$ is the vector of the probability current. Equations (6a),(6b) are equivalent to those defining the ψ potential in Ref. [16].

Note that if χ were a solution of a problem with a real local potential, then, because of $W \equiv 0$, the current would be free of divergence. However, W for a nonlocal problem does not vanish; a nonlocal potential pumps flux from one location to another.

By analogy with Eq. (5), one can define a TELP for each partial wave:

$$U_l(r) = [\chi_l(r)]^{-1} v_l \chi_l(r), \tag{7}$$

where $\chi_l(r)$ and v_l are the l partial-wave components of $\chi(\mathbf{r})$ and v, respectively. Clearly, $U_l(r)$ is both l dependent and energy dependent and will be singular at nodes of $\chi_l(r)$, but it is real and isotropic. One can generalize to an lj-dependent radial function, χ_{lj}.

In short, we can form *either* a TELP depending on direction *or* an l-dependent TELP. We find more information in the former, particularly in view of the singularity of the latter for certain partial waves.

IV. INVERSION PROCEDURE

The singularity of the l-dependent TELP's means they cannot be compared with phenomenological single-body local potentials, or applied to models of mass-6 nuclei, for example. Local potentials $V(r)$ that reproduce the microscopic phase shifts δ_{lj} (equivalently, $S_{lj} = \exp 2i\delta_{lj}$) can be obtained by applying $S_{lj} \rightarrow V(r)$ inversion. There exists a suitable spin half inversion procedure: the iterative-perturbative (IP) method implemented in the code IMAGO [17]. The extension from the more usual "fixed energy" inversion to "mixed-case" inversion, which yields a potential reproducing phase shifts δ_{lj} for a limited set of partial waves over a limited energy range, was introduced in Ref. [2]. A discussion of IP inversion and its application can be found in Ref. [18]. In mixed-case inversion, particular subsets of partial waves may be included, for example, to produce either energy-independent l-dependent potentials or energy-dependent l-independent potentials, subject to the limits of the available δ_{lj}. Here we closely follow the techniques developed in Ref. [1], based on the concept of "energy bites." The idea is to invert S_{lj} for a set of closely spaced energies. This yields a potential which gives both the mean value of S_{lj} across the energy interval, but also reproduces the energy dependence of S_{lj} across the interval. It is essential to incorporate, in this manner, information concerning the energy dependence of δ_{lj} in order to stabilize what is effectively fixed-energy inversion in a regime where few phase shifts significantly differ from zero. In Ref. [1], these techniques yielded energy- and parity-dependent potentials from empirical δ_{lj} for low-energy $\alpha + p$ scattering.

The IP method has been described before and we only note relevant points and definitions. The algorithm iteratively corrects a "starting reference potential" by adding a linear superposition of basis functions. Since the calculations presented here are obtained with a very small basis, we expect some sensitivity to the choice of the basis. This parameter dependence is assessed using alternative bases. The quality of an inversion is quantified by the "phase-shift distance" σ. This is defined in terms of the target phase shifts $\{\delta^T_{lj}(E)\}$, for which we seek the underlying potential, and the phase shifts $\{\delta^I_{lj}(E)\}$ calculated from that potential found by inversion, as follows:

$$\sigma^2 = \sum_{l,j,E} \left|\exp[2i\delta^T_{lj}(E)] - \exp[2i\delta^I_{lj}(E)]\right|^2, \tag{8}$$

where the sum is over all required l, j values and over all values of E defined in the energy bite.

Even with the techniques outlined above, the fact that there are at most four contributing l values implies that one must use a relatively small inversion basis. To minimize consequent ambiguities, we accept the smoothest possible potential and, in the case of energy-dependent potentials, a regular energy dependence. Inversion can lead to potentials with oscillatory features; these features can be due to an underlying l dependence or nonlocality, but might also simply be artifacts of the inversion procedure. We have reduced the presence of such artifacts by a simple smoothing procedure, described in Ref. [1], involving the imposition of exponential tails. If such smoothing does not lead to converged smooth potentials, we infer that the oscillations are necessary to fit the given set of partial waves. Characteristically, δ_{lj} derived from l-dependent or energy-dependent potentials correspond to oscillatory local potentials.

The proton inversions involve the standard optical model Coulomb potential based on a uniform spherical charge (radius $1.3 \times 4^{1/3}$ fm), facilitating the subsequent use of our potentials in optical model codes. Our proton potentials are thus subject to a small correction near the nuclear surface equal to the difference between conventional and exact Coulomb potentials. All inversions were performed with a matching radius of 8 fm.

V. RESULTS

A. Microscopic phase shifts

The phase shifts δ_{lj} obtained from the RGM CC and SC calculations are presented in Fig. 1 and Fig. 2 as functions of energy (all energies quoted are for the laboratory frame) together with empirical phase shifts corresponding to both effective-range [19] and R-matrix parametrized [20] fits to the data. The degree of uncertainty associated with empirical δ_{lj} may be inferred by comparing these latter two sets. Potentials found by inversion corresponding to these experimental phase shifts

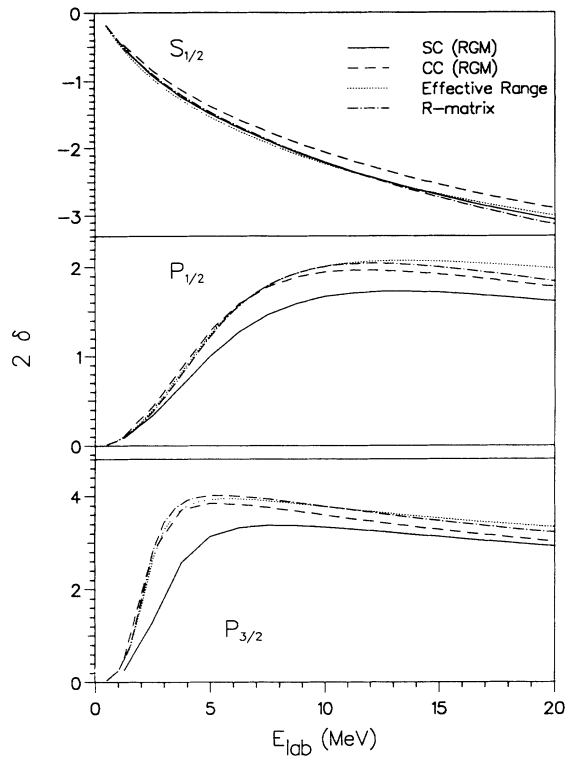

FIG. 1. Twice the phase shift in radians for S waves and P waves for $\alpha + p$ scattering, comparing RGM and empirical solutions. The solid and dashed lines are the SC and CC RGM phase shifts, respectively, and the dotted and dot-dashed lines are the effective-range and R-matrix fits, respectively.

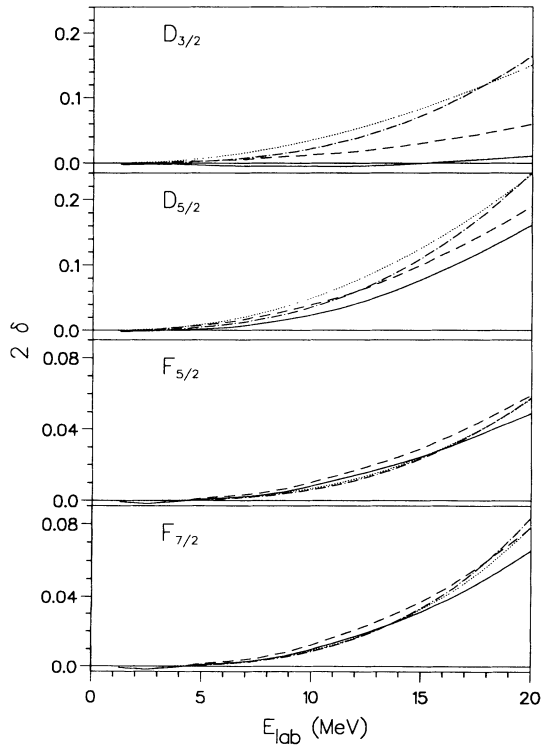

FIG. 2. Twice the D-wave and F-wave phase shifts, otherwise as for Fig. 1.

have been determined [1]. Uncertainties in such empirical potentials reside in ambiguities in empirical S_{lj} and not in the $\delta_{lj} \rightarrow V(r)$ inversion.

The SC and CC δ_{lj} are mostly within a few degrees of the empirical δ_{lj}, with roughly the correct energy dependence. The changes in δ_{lj} generated by the channel coupling differ from case to case. For S waves, the SC phase shifts happen to correspond more closely to the empirical values, whereas the P-wave resonances are only reproduced well when coupling is included. The phase shifts for the D and F waves are much smaller and are also less well known empirically. The influence of channel coupling is strongest in the $D_{3/2}$ phase shift obviously because of the prominent $\frac{3}{2}^+$ resonance just beyond the $h+d$ threshold. The relatively poor description of the $D_{3/2}$ phase shifts reflects the fact that the RGM calculation puts the $h + d$ threshold, and with that, the resonance, some 2.5 MeV too high. Overall, the $h + d$ channel appears to be essential for $p + \alpha$ scattering.

The RGM phase shifts were evaluated at intervals of 0.25 MeV. However, inversion requires phase shifts at much more closely spaced energies so that both D and F waves contribute; otherwise the larger energy gradients of δ_{lj} for lower l dominate the inversion. To optimize the choice of energy bites [1], the RGM δ_{lj} were parametrized by an effective-range expansion following the prescription of Schwandt *et al.* [19] with the correction for Coulomb barrier penetration. For all but the P waves, requiring four parameters, the energy dependence could be fitted with two parameters. The resulting fit to the RGM phase shifts was very close: The differences are only discernible on graphs of the scale of Fig. 2 for the F waves for $E_{\rm lab} <$ 10 MeV. That is the estimated numerical accuracy of the RGM calculations.

B. Inversion potentials

We have applied inversion to both the SC and the CC phase shifts for $\alpha + p$ as well as $\alpha + n$ scattering. Below we present results mainly for $\alpha + p$ scattering since the $\alpha + n$ results were very similar.

In successive subsections we describe two ways of inverting the phase shifts to define potentials: (1) establish potentials corresponding to particular energies and (2) establish potentials fitting particular partial waves, or small sets of partial waves, over the entire sub-threshold energy range.

The first class of potentials is of immediate interest to phenomenology and enables one to compare the energy dependence of the RGM-derived potentials with both phenomenological systematics and the empirical potentials [1]. Since both the nucleon-nucleon force and the nonlocal microscopic potential v are energy independent, any energy dependence is a property of local equivalents to nonlocal potentials, and to channel coupling in the CC case. We comment below on the consequences for nucleon scattering from heavier nuclei.

The second class of potentials provide useful comparisons with Ref. [1] and yield, through the examination of charge symmetry properties, a useful test of the methods.

1. *Potentials for laboratory energies of 12 MeV and 18 MeV*

Potentials have been established using mixed-case inversion for laboratory energies of 12 and 18 MeV. More specifically, these energies were the centers of narrow energy bites, 12 ± 0.03 MeV and 18 ± 0.03 MeV.

We find that any potential which simultaneously fits S_{lj} for all l behaves in an unphysical manner at large r, extending out much further than would be expected and exhibiting a change in sign. See Fig. 3 for the CC case. Just this general property was found in the "all-l" fits to the empirical phase shifts [1]. The energy dependence of the potentials apparent in Fig. 3 appears reasonable for most r, but we shall see below that the "volume integrals" show an anomalous contrary dependence.

Using the same procedure we determined *parity-dependent* potentials at 12 and 18 MeV. That is, we find pairs of potentials which reproduce the values and energy dependence of, respectively, the odd and even partial-wave phase shifts at these energies. The parity-dependent potentials *do* behave reasonably in the surface and we present the CC results in Fig. 4. The odd and even potentials have very different radial forms, the odd-parity term having a much longer range, and crossing over the even parity term which is deeper at $r = 0$. This is just the behavior of the empirical potential [1]. In Fig. 5 we express the central potential in the form $V_1(r) + (-1)^l V_2(r)$ and compare V_1 and V_2 for the 12 MeV CC and SC RGM potentials with the same quantities for empirical potentials. We see that the channel coupling brings closer agreement, so that the CC V_1 agrees

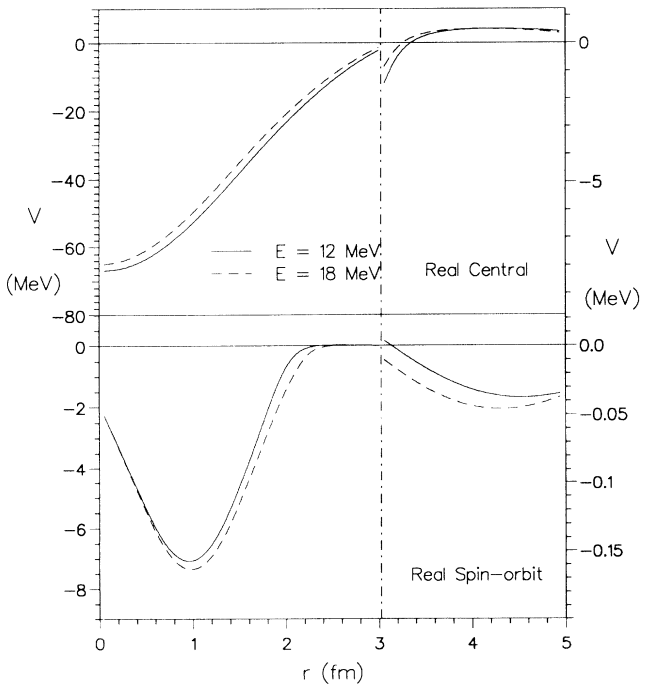

FIG. 3. The central and spin-orbit $\alpha + p$ potentials fitting all partial waves, the "all-l solutions," obtained by inverting 12 MeV (solid) and 18 MeV (dashed) RGM CC phase shifts. Note the expanded scale in the surface region.

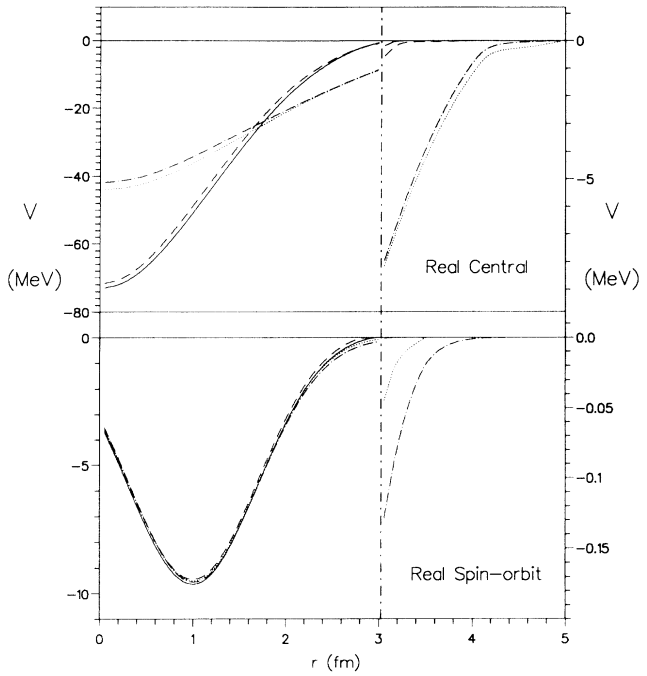

FIG. 4. The central and spin-orbit $\alpha + p$ potentials fitting odd and even partial waves separately, obtained by inverting 12 MeV and 18 MeV RGM CC phase shifts. Solid line, 12 MeV, even; dashed line, 18 MeV, even; dotted lines 12 MeV, odd; dot-dashed line, 18 MeV, odd.

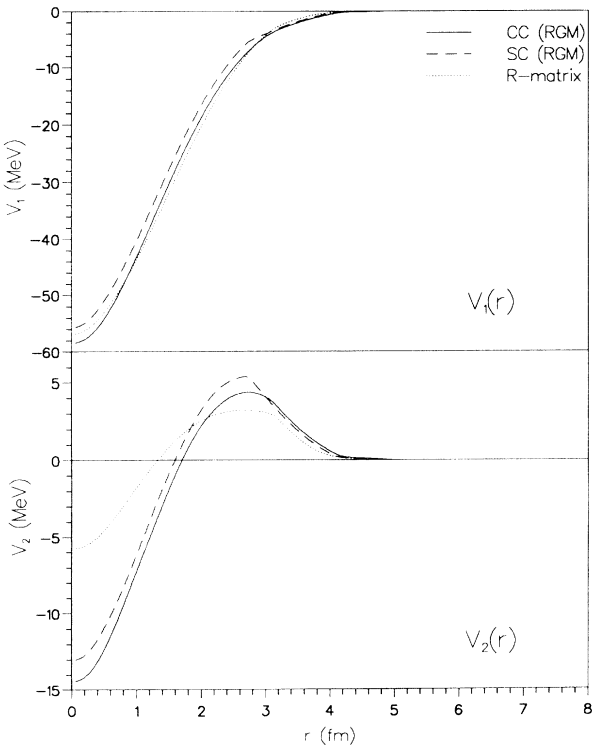

FIG. 5. Comparison of the terms V_1, V_2 of the central $\alpha + p$ potentials expressed as $V_1 + (-)^l V_2$, at 12 MeV. RGM CC (solid line), RGM SC (dashed line), the potential inverted from the empirical R matrix (dotted line).

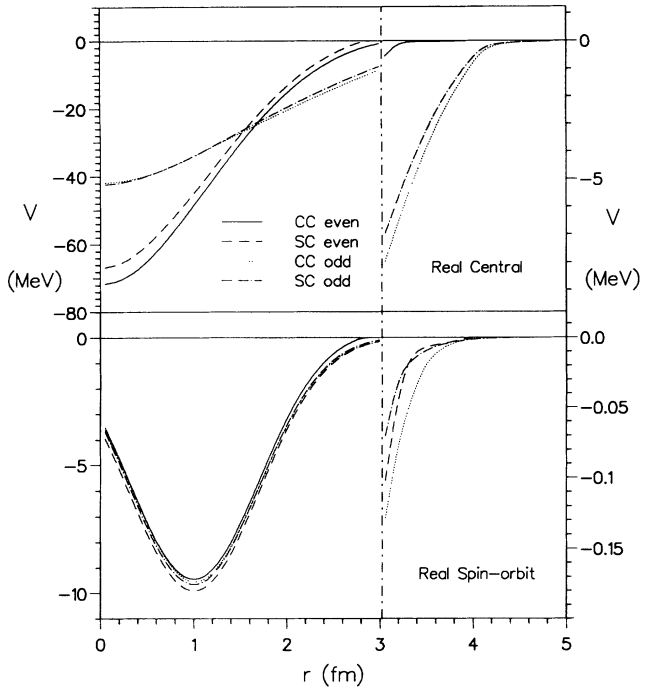

FIG. 6. Proton-α central (above) and spin-orbit (below) potentials, showing the effect of channel coupling at 18 MeV. The solid line shows CC even, the dashed line the SC even, the dotted line the CC odd, and the dot-dashed line the SC odd potentials.

remarkably well with the empirical V_1. The qualitative nature of the RGM V_2 is the same as for the empirical V_2, although the magnitude is greater. Although Fig. 5 shows only one empirical potential, the R-matrix and effective-range empirical potentials closely agree.

Referring back to Fig. 4, we see that for $r < 3$ fm both the odd-parity and even-parity potentials fall with increasing energy much as would be expected from nucleon-nucleus systematics. The spin-orbit potential peaks at about 1 fm, a universal property of all the inverted potentials, and also a general property of nucleon-nucleus potentials. However, the spin-orbit term is much less well determined than the central term, especially for D waves.

As required, the even-parity potentials support a single $l = 0$ bound state. For the potential fitting the 12 MeV phase shifts, this is at $E = -8.38$ MeV (SC case) or at $E = -11.675$ MeV (CC case). The odd-parity potentials support none. This $l = 0$ state corresponds to the single Pauli-forbidden state, and its appearance shows that our potential tallies with those calculated directly from the RGM kernels [21,22]. The potentials we exhibit therefore do belong to the same family as "the true" potentials, and not to families of their supersymmetric partners [23–25].

Figure 6 compares the full CC 18 MeV RGM potentials with those for the SC RGM at the same energy. It can be seen that coupling to the $h + d$ channels induces a substantial *attractive* effect in the even-parity potential for all r, consistent with the deeper bound state noted above. The effect on the even-parity potential is probably magnified by the $\frac{3}{2}^+$ resonance.

The energy dependence of the potentials is conveniently quantified in terms of the volume integral J_R and rms radius which also facilitate comparison with wider nucleon-nucleus phenomenology [26]. Table I presents these characteristics. The "all-l" volume integrals and, especially, rms radii must be treated with caution because of the large-r behavior of these potentials. With this proviso, we note that the energy dependence of the "all-l" volume integral is of the wrong sign again in striking conformity with the corresponding empirical potentials [1].

Table I also suggests that the effect of channel coupling on the odd-parity solutions is almost as large as for the even-parity potentials; this is not what might appear to be the case in Fig. 6. This is also a "large-r" effect, since closer examination of Fig. 6 reveals that indeed coupling does have a notable effect on the tail ($r > 3$ fm) of the odd-parity potential. It is the "all-l" volume integrals which approach the values expected for heavy nuclei. The parity dependence of the nucleon-nucleus optical potential is small for heavy nuclei and it is remarkable that J_R for such nuclei is roughly the mean of the odd and even

TABLE I. Volume integrals J_R and rms radii for potentials found by mixed-case inversion at 12 MeV and 18 MeV (laboratory) Characteristics of potentials inverted from CC and SC phase shifts are shown for the two components of the parity-dependent solutions as well as for the "all-l" potentials.

		Even l		Odd l		All l	
Energy (MeV)	SC/CC	J_R (MeV fm^3)	$\langle r^2\rangle^{1/2}$ (fm)	J_R (MeV fm^3)	$\langle r^2\rangle^{1/2}$ (fm)	J_R (MeV fm^3)	$\langle r^2\rangle^{1/2}$ (fm)
			Central potential				
12	CC	366.9	1.729	657.7	2.516	474.9	2.242
12	SC	290.5	1.595	607.7	2.474	-	-
18	CC	347.4	1.744	620.1	2.460	479.1	3.183
18	SC	289.9	1.629	570.6	2.410	-	-
			Spin-orbit potential				
12	CC	68.1	1.653	69.0	1.686	35.2	1.829
12	SC	73.5	1.713	69.9	1.689	-	-
18	CC	64.4	1.623	72.5	1.743	41.1	1.420
18	SC	74.8	1.727	71.2	1.708	-	-

values for ^{4}He.

Finally, Table I suggests that when the entire radial range is considered, it is only when coupling is included that the even-parity potential falls with energy in the expected fashion.

The striking result is that the RGM δ_{lj} yield a potential with the highly characteristic parity-dependent radial form found by inverting empirical δ_{lj}. It is also satisfying that the RGM plus inversion has led to such details as the correct energy dependence, the spin-orbit potential peaking at a smaller radius than the halfway point of the central potential (a universal phenomenological property), J_R consistent with heavy nuclei, and a plausible channel-coupling effect.

2. *Potentials fitting all energies*

Potentials can be derived which fit the phase shifts for any l value, i.e., for each pair $(l, j = l + \frac{1}{2})$ and $(l, j = l - \frac{1}{2})$ for the energy range 0–20 MeV. In this way we find potentials that are particularly well determined by the $l = 1$ resonances. Fitting the energy-dependent phase shifts for other lj yields less well-defined potentials although differences between SC and CC potentials emerge which are independent of the inversion basis.

The CC and the SC $l = 1$ α-p potentials are similar to the empirical potentials shown in Fig. 6 of Ref. [1]. The CC potential is more attractive than the SC potential for $r > 1.8$ fm and less attractive for small r and the same is found for $\alpha+n$. (In Fig. 6 the odd-parity potential shows a similar but weaker crossover in the sign of the coupling effect, with attraction at larger radii.) Differences between the $l = 1$ proton and neutron SC potentials are very small and for the CC potentials scarcely visible on a plot. Although a direct consequence of charge symmetry which is built into the RGM calculations (in contrast to the empirical case [1], where charge symmetry emerged from the experimental data), it is significant. Since the Coulomb force is strong enough to put the P-wave resonances at different energies for protons and neutrons, the emergence of precisely charge-symmetric potentials confirms the correctness of the overall RGM plus inversion calculations.

We find that representation by smooth parity-dependent potentials requires a separate potential for each energy since any parity-dependent potential fitting all energies will have some degree of surface oscillation. A local potential fitting phase shifts which embody *either* l dependence *or* energy dependence will be oscillatory in some degree.

C. Perey factors and trivially equivalent potentials

Local α-nucleon potentials are applied in, for example, three-body models of ^{6}Li [27] and of ^{6}He [28]. To evaluate such models, one must measure the importance of nonlocality. An estimate can be found by comparing RGM wave functions with those for the δ_{lj}-equivalent local, but possibly l-dependent, potential.

For the SC calculation we introduce a generalized Perey factor [4]. The wave functions for the equivalent local potential, $\chi^{\rm local}(\mathbf{r})$, follow from the Schrödinger equation with local potentials found by inversion. We then define the generalized Perey factor:

$$R(\mathbf{r}) = \frac{|\chi(\mathbf{r})|}{|\chi^{\rm local}(\mathbf{r})|}. \tag{9}$$

We present the ratio $R(\mathbf{r})$ on the scattering plane in Fig. 7 for 18 MeV protons, with SC χ and $\chi^{\rm local}$ of the parity-dependent inversion potential. In this figure the particle flux comes from the left, with the impact parameter represented by the vertical axis. The pattern is up-down asymmetric due to the spin-orbit force; the ratio is presented for the nucleon spin projection normal outwards from the plane of the paper.

The function R varies widely, from < 0.7 to > 1.2. While there is a strong Perey-like effect ($R < 1$) close to the center, there are also conspicuous regions where the nonlocal wave function has considerably the greater magnitude ("anti-Perey" effect). At lower energies the pattern is similar but slightly greater in range. $R(\mathbf{r})$ calculated with the wave function for the 18 MeV l-independent potential (see Fig. 3) in the denominator varies much more widely having with both $R < 1$ and $R > 1$ regions extending to greater radii; however, the "Perey" region almost completely covers the region of

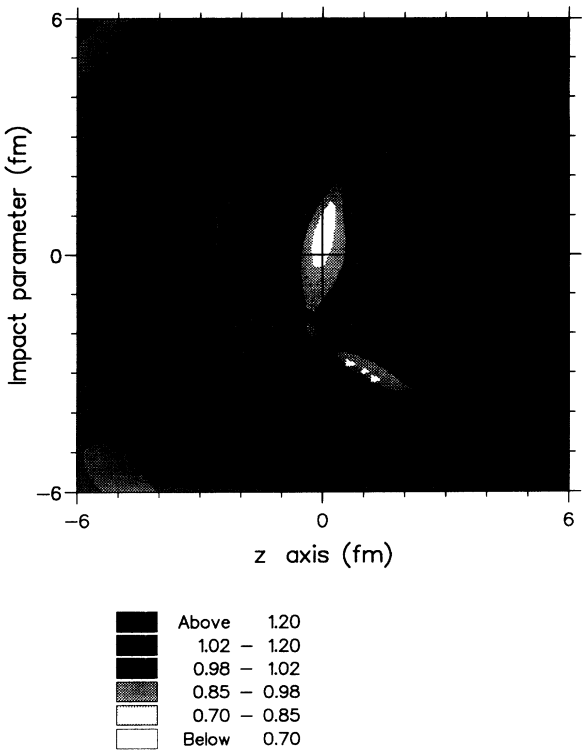

FIG. 7. Ratio of the magnitudes of the RGM SC wave function χ and of the wave function for the parity-dependent inverted potential for 18 MeV protons. The figure represents the scattering plane, with the nuclear center at the center, the impact parameter plotted vertically, and the protons incident from the left. The asymmetry between the positive and negative impact parameters reflects the fact that the nucleon spin is normal to the page.

nuclear overlap.

Since there are few partial waves, one can compare wave functions for each lj individually. In Fig. 8 the functions $|\chi_{lj}(r)|$ are compared with $|\chi_{lj}^{\text{parity}}(r)|$ and $|\chi_{lj}^{l\text{-indep}}(r)|$ calculated from the parity-dependent and l-independent potentials, respectively, for some of the partial waves. As expected from the remarks above, $\chi^{l\text{-indep}}$ differs much more from χ than χ^{parity}. The largest difference between $|\chi_{lj}(r)|$ and $|\chi_{lj}^{\text{parity}}(r)|$ is seen for the S wave for $r < 2$ fm, corresponding to the Perey-like effect at the nuclear center in Fig. 7. Projecting the Pauli-forbidden state out of χ^{parity} for $l = 0$ brings it somewhat closer to the RGM wave function for $r < 1.5$ fm, but somewhat increases the difference beyond that radius. One sees from Fig. 8 that there is a general, but not universal, tendency for the RGM wave function to be damped relative to the wave function of the preferred (parity-dependent) local potential.

What we see in Fig. 7 is very different from the conventional Perey damping. Both a parity-dependent local potential and an l-independent nonlocal potential give rise to strong damping (or antidamping) effects on a wave function when compared to the respective phase-shift-equivalent l-independent local potentials. We shall now argue that the wave functions χ do embody strong nonlocal effects beyond those due to parity dependence. The argument hinges upon the properties of the imaginary ψ potential defined in Eq. (6b). In Fig. 9 we present this quantity on the scattering plane for the 18 MeV RGM SC wave functions. The quantity is not calculated beyond $r = 8$ fm, the matching radius. We see that this quantity differs considerably from zero, although the asymptotic flux is conserved exactly. A nonlocal potential removes flux from certain regions, reemitting it elsewhere — hence the balance of absorptive and emissive regions in this figure. This does not, however, suffice to demonstrate the effect of nonlocality on each partial-wave component of the wave function. The argument has to be more subtle since even a purely real, local, parity-dependent potential gives a ψ potential with strong emissive and absorptive regions. For example, we show in Fig. 10 the imaginary ψ potential constructed with the wave function of the 18 MeV SC parity-dependent local potential. It is very different from Fig. 9. The approximate antisymmetry about $z = 0$ is meaningful, as will now be discussed.

There is a striking property of $\nabla \cdot \mathbf{j}$: It is not hard to show, starting from Eq. (10) of Ref. [16] and assuming no spin-orbit potential that a parity-dependent potential, $V_1(r) + (-1)^l V_2(r)$, which is *local for each partial wave*, will lead to $\nabla \cdot \mathbf{j}(\mathbf{r})$ having the form

$$\nabla \cdot \mathbf{j}(\mathbf{r}) = \alpha \sum_{\text{odd } l} Z_l(r) Y_{l0}(\theta), \tag{10}$$

which has precise odd symmetry about the $z = 0$ plane. A consequence is that the imaginary ψ potential should

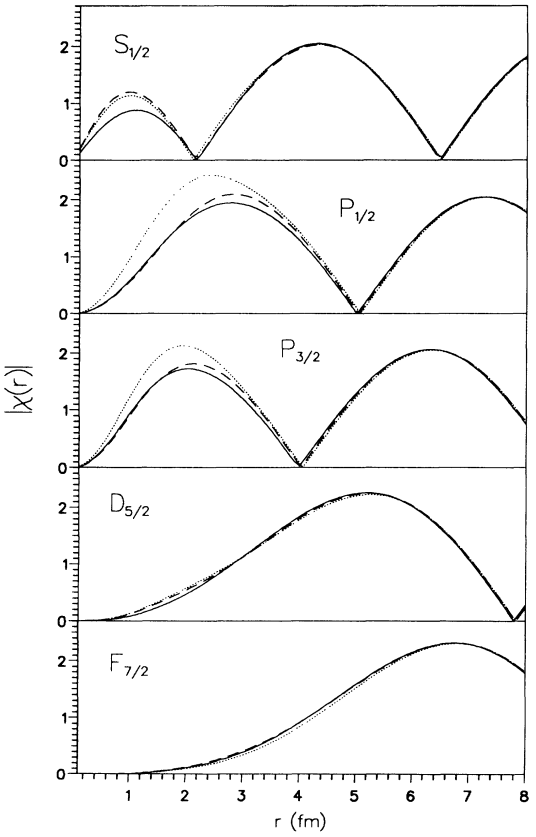

FIG. 8. For selected partial waves of 18 MeV protons, the magnitude of the RGM radial wave function χ_{lj} (solid line) compared with magnitudes of wave functions calculated from the parity-dependent (dashed line) and l-independent (dotted line) phase-equivalent potentials.

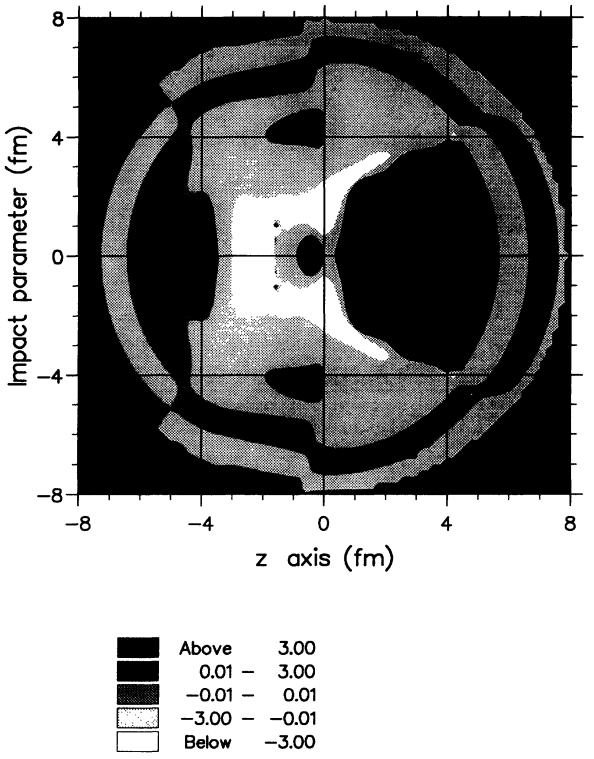

FIG. 9. The imaginary ψ potential for the 18 MeV RGM SC calculation plotted on the scattering plane as in Fig. 7.

exhibit a similar property but modulated by the variation of $|\chi|$ over the reaction plane. The pattern of positive and negative regions will be unaffected by variations in $|\chi|$ and must show exact antisymmetry, although the actual magnitude of the imaginary ψ potential will not. We have confirmed this for the imaginary ψ potential calculated from the parity-dependent inversion potentials using judicious contour lines: The regions for which it is, respectively, $> 10^{-5}$ and $< -10^{-5}$ are precise reflections of each other in the $z = 0$ plane, but the detailed "hills and valleys" are only approximate reflections. In fact, this is more than might have been expected, since the derivation of Eq. (10) assumes that there is no spin-orbit force, and, indeed, $\nabla \cdot \mathbf{j}$ is far from antisymmetric about $z = 0$ for a parity-dependent potential with spin-orbit term. However, the spin-orbit force also twists the pattern of $|\chi|$ (for a nucleon with spin quantized normal to the scattering plane), so that it differs between the regions of positive and negative impact parameters; for the parity-dependent inversion potential the quantity evaluated from Eq. (6b) does have exact antisymmetry in sign and approximate antisymmetry in magnitude.

Why do RGM χ wave functions not yield imaginary ψ potentials exhibiting clear antisymmetry about $z = 0$? In Fig. 9, approximate antisymmetry can be seen for $6 < r < 8$ fm but not for $r < 6$ fm. The explanation is that the RGM kernels are not only effectively parity dependent, but also highly nonlocal, partial wave by partial wave. (We stress this because l dependence is sometimes misleadingly called an effective nonlocality.) Thus,

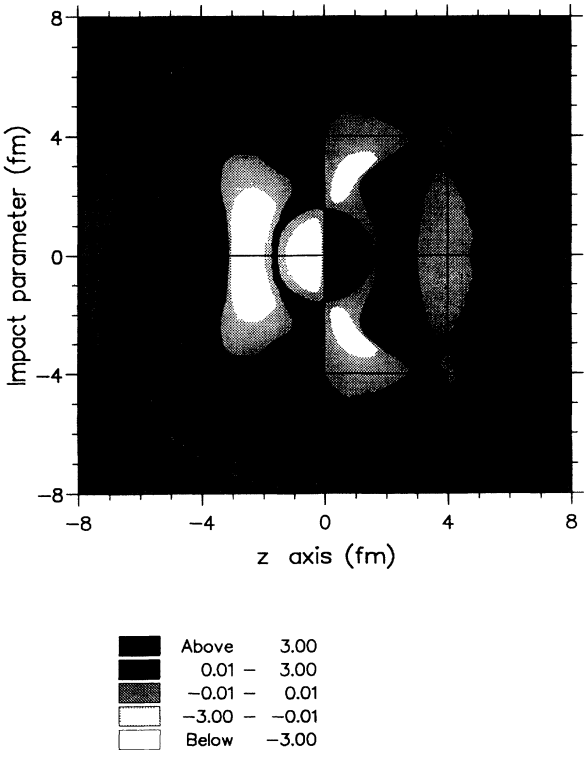

FIG. 10. The imaginary ψ potential for the parity-dependent potential fitting the phase shifts of the 18 MeV RGM SC calculation, plotted on the scattering plane as in Fig. 9.

inspection of the imaginary ψ potential immediately reveals the nonlocality partial wave by partial wave, an effect in addition to parity dependence. It is worth mentioning that we found the partial-wave TELP's erratically angular momentum dependent.

In consequence, any use of RGM local potentials in applications must allow for the fact that nonlocal effects are strong and are *not* allowed for by using parity-dependent potentials, although indeed they must be parity dependent.

All nonlocality evident in these comparisons between the wave functions of the RGM and of its local equivalents are due to the exchange effects inherent in the RGM. There is an additional nonlocality due to channel coupling, but accurate study requires the second channel to be orthogonalized to the elastic channel [29]. Since our RGM is not orthogonalized, we have only studied the SC case here.

VI. DISCUSSION AND CONCLUSIONS

In many ways, the RGM provides the most complete framework for calculating reactions between nuclei. Antisymmetrization, which plays a crucial role, can be included exactly alongside channel-coupling effects. Nevertheless, the RGM is an approximation requiring not only basis truncation but also effective nucleon-nucleon potentials. For computability, these interactions tend to be of simple functional forms, but they have no strict theoretical foundation. Therefore the superiority of the RGM over simpler approaches, such as the folding model, is not unqualified, and elaborations of the folding model are far more feasible for complex nuclei. It is for this reason that these light nucleus studies can contribute to our more general understanding of nucleon-nucleus interactions, with the systematics of local potentials playing a key role, since local potentials are still at the center of single-body models, including modern efforts [30] to unify shell and optical models.

Currently, the most useful model for nucleon-nucleus potentials for heavier nuclei is a local folding model with effective interactions based on local-density G-matrix theory and a crude representation of antisymmetrization; this certainly misses aspects that the RGM encompasses, parity dependence being an example. It has long been known that RGM calculations predict parity dependence, but this has been very hard to pin down empirically. The quality of fit to the scattering data is such that a wide variety of phenomenological potentials, with and without parity dependence, give fits of comparable mediocre quality. Indeed, conventional phenomenology has failed to give a decisive answer on the existence of parity dependence for very light systems, although the argument for heavier cases such as ^{4}He on ^{20}Ne [31] is more convincing. For $\alpha + p$ scattering, there is insufficient information in the single energy angular distributions to establish parity dependence decisively, particularly since there has been no motivation to adopt a parametrization other than a $1+c(-1)^l$ multiplicative factor. However, by using inversion methods which include information from the energy dependence of the phase shifts, we established [1] from

experimental data that the $\alpha + p$ interaction *was* parity dependent but *not* with an overall $1 + c(-1)^l$ factor.

By applying inversion to RGM phase shifts, we find the *same* form of parity dependence as had been deduced from experiment; see Fig. 5. That is, we have established that the RGM predicts a form of parity dependence which, unusual as it is, is required by experiment. We emphasize that this has been established independently of the degree to which the RGM fits experiment directly and hence is not contingent upon the choice of effective nucleon-nucleon interaction. Figure 5 also shows that the present RGM CC calculation leads to a potential whose parity-independent component is remarkably close to that required by data.

Concerning empirical parity dependence in general, we see that one should parametrize using the general form $V_1(r) + (-1)^l V_2(r)$ and not an overall $1 + c(-1)^l$ multiplicative factor. Indeed, what we found [2] for ^{12}C+α scattering is very similar to the pattern of Fig. 5. This suggests that a longer-ranged odd-parity component is a general property.

Local potentials have many applications beyond parametrizing scattering data. If we are to attribute any meaning to the wave functions they produce, it is important to explore their relationship to the RGM wave functions. For this reason we have presented "Perey" factors, and compared our inversion potentials with trivially equivalent local potentials.

It was found that the local potentials produce wave functions which agree in broad features but differ in details appreciably from the RGM relative wave function χ. The difference is certainly reduced if the macroscopic model is changed so that its equation of motion may include Pauli projection [14]. But the moderate agreement of the wave functions in the P waves shows that refinements beyond the exclusion of forbidden states may be required.

We have seen that nonlocality has effects beyond the so-called Perey effect. This needs to be understood since local potentials continue to be useful in a range of structure and reaction calculations, as phenomenological tools in reproducing scattering data and in establishing the link between nuclear reactions and structure [30]. They also provide a link between experiment and microscopic calculations, as the present work has shown. The nonlocality is in addition to effects of parity dependence, although this happens to be also related to exchange.

Although strongly parity dependent, the nucleon-α potential is consistent with the systematic behavior of the general nucleon-nucleus potential in a particular sense. The key point is that although the volume integral of the odd component for $p, n + \alpha$ is much larger than predicted by systematics for heavy nuclei and conversely the volume integral of the even component is smaller, neverthless, the average of the two closely conforms to systematics.

ACKNOWLEDGMENTS

This work was supported by OTKA Grant No. 3010 (Hungary) and by SERC Grant No. GR/G01522 (UK).

[1] S. G. Cooper and R. S. Mackintosh, Phys. Rev. C **43**, 1001 (1991).
[2] S. G. Cooper and R. S. Mackintosh, Nucl. Phys. **A517**, 285 (1990).
[3] S. G. Cooper and R. S. Mackintosh, Inverse Prob. **5**, 707 (1989).
[4] S. G. Cooper and R. S. Mackintosh, Nucl. Phys. **A511**, 29 (1990).
[5] S. G. Cooper and R. S. Mackintosh, Nucl. Phys. **A513**, 373 (1990).
[6] S. G. Cooper and R. S. Mackintosh, Z. Phys. A **337**, 357 (1990).
[7] A. Csótó, R. G. Lovas, and A. T. Kruppa, Phys. Rev. Lett. **70**, 1389 (1993).
[8] G. Blüge and K. Langanke, Phys. Rev. C **41**, 1191 (1990).
[9] G. Blüge and K. Langanke, Few-Body Syst. **11**, 137 (1991).
[10] F. S. Chwieroth, Y. C. Tang, and D. R. Thompson, Phys. Rev. C **9**, 56 (1974).
[11] I. Reichstein and Y. C. Tang, Nucl. Phys. **A158**, 529 (1970).
[12] P. Heiss and H. H. Hackenbroich, Phys. Lett. **30B**, 373 (1969).
[13] K. F. Pál, R. G. Lovas, M. A. Nagarajan, B. Gyarmati, and T. Vertse, Nucl. Phys. **A402**, 114 (1983).
[14] See, e.g., S. Saito, Prog. Theor. Phys. Suppl. **62**, 11 (1977).
[15] S. G. Cooper, R. S. Mackintosh, A. Csótó, and R. G. Lovas, Open University Report No. OUPD9314, 1993.
[16] R. S. Mackintosh, A. A. Ioannides, and S. G. Cooper, Nucl. Phys. **A483**, 173 (1988).
[17] S. G. Cooper and R. S. Mackintosh, User's manual for IMAGO, Report No. OUPD9201, 1992.
[18] R. S. Mackintosh and S. G. Cooper, in *Quantum Inversion Theory and Applications, Proceedings, Bad Honnef*, edited by H. V. von Geramb (Springer-Verlag, Berlin, 1994).
[19] P. Schwandt, T. B. Clegg, and W. Haeberli, Nucl. Phys. **A163**, 432 (1971).
[20] Th. Stammbach and R. L. Walter, Nucl. Phys. **A180**, 225 (1972).
[21] H. Friedrich, Phys. Rep. **74**, 210 (1981).
[22] H. Horiuchi, *Trends in Nuclear Physics*, edited by P. J. Ellis and Y. C. Tang (Addison-Wesley, New York, 1991), Vol. 2, p. 277.
[23] D. Baye, in [18].
[24] D. Baye, Phys. Rev. Lett. **58**, 2738 (1987).
[25] Q. K. K. Liu, in [18].
[26] G. R. Satchler, *Direct Nuclear Reactions* (Oxford University Press, Oxford, 1983).
[27] N. W. Schellingerhout, L. P. Kok, S. A. Coon, and R. M. Adam, Phys. Rev. C **48**, 2714 (1993).
[28] M. V. Zhukov, B. V. Danilin, A. A. Korsheninnikov, D. V. Fedorov, L. V. Chulkov, J. S. Vaagen, and J. M. Bang,

in *Proceedings of the International Symposium on Structure and Reactions of Unstable Nuclei, Niigata, 1991*, edited by K. Ikeda and Y. Suzuki (World Scientific, Singapore, 1991), p. 158.

[29] E. Schmid and G. Spitz, Z. Phys. A **321**, 581 (1985).
[30] C. Mahaux and R. Sartor, Adv. Nucl. Phys. **20**, 1 (1991)
[31] F. Michel and G. Reidemeister, Z. Phys. A **333**, 331 (1989).

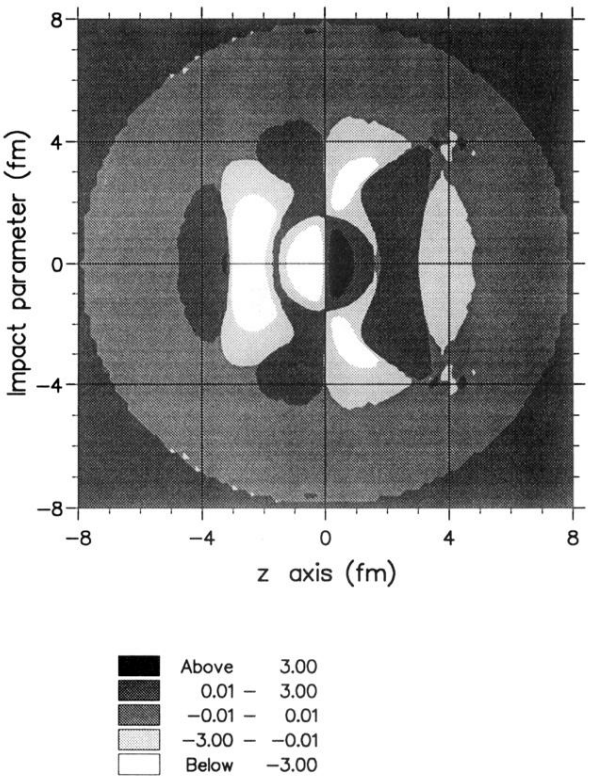

FIG. 10. The imaginary ψ potential for the parity-dependent potential fitting the phase shifts of the 18 MeV RGM SC calculation, plotted on the scattering plane as in Fig. 9.

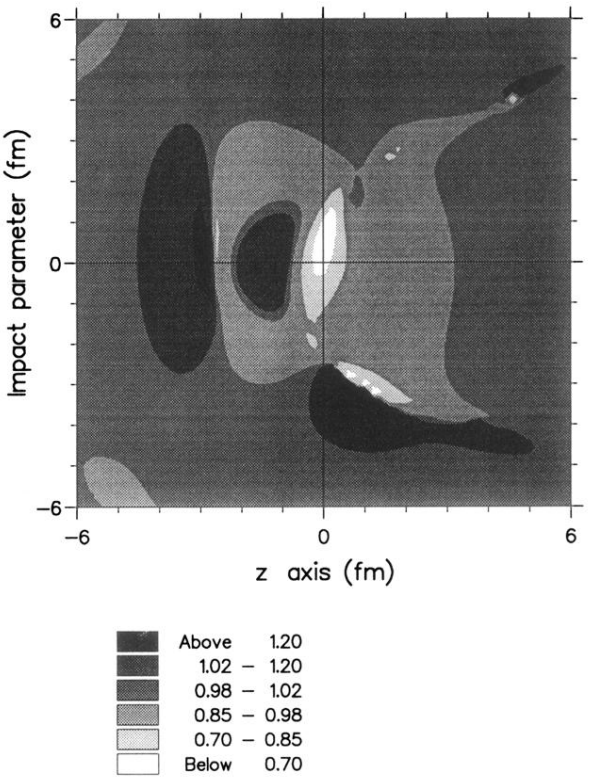

FIG. 7. Ratio of the magnitudes of the RGM SC wave function χ and of the wave function for the parity-dependent inverted potential for 18 MeV protons. The figure represents the scattering plane, with the nuclear center at the center, the impact parameter plotted vertically, and the protons incident from the left. The asymmetry between the positive and negative impact parameters reflects the fact that the nucleon spin is normal to the page.

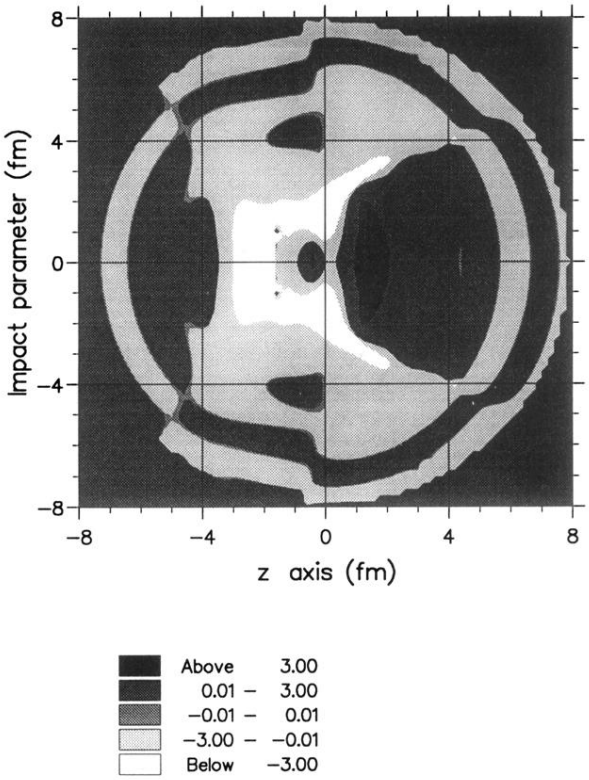

FIG. 9. The imaginary ψ potential for the 18 MeV RGM SC calculation plotted on the scattering plane as in Fig. 7.